JACS
JOURNAL OF THE AMERICAN CHEMICAL SOCIETY
Article
pubs.acs.org/JACS

Beyond Entropy: Magnetic Forces Induce Formation of Quasicrystalline Structure in Binary Nanocrystal Superlattices

Zhijie Yang,[†,‡] Jingjing Wei,[†,‡] Pierre Bonville,[§] and Marie-Paule Pileni*[,†,‡,§]

[†]Sorbonne Universités, UPMC Univ Paris 06, UMR 8233, MONARIS, F-75005, Paris, France
[‡]CNRS, UMR 8233, MONARIS, F-75005, Paris, France
[§]CEA/IRAMIS, CEA Saclay, 91191, Gif-sur-Yvette, France

Supporting Information

ABSTRACT: Here, it is shown that binary superlattices of Co/Ag nanocrystals with the same size, surface coating, differing by their type of crystallinity are governed by Co−Co magnetic interactions. By using 9 nm amorphous-phase Co nanocrystals and 4 nm polycrystalline Ag nanocrystals at 25 °C, triangle-shaped NaCl-type binary nanocrystal superlattices are produced driven by the entropic force, maximizing the packing density. By contrast, using ferromagnetic 9 nm single domain (*hcp*) Co nanocrystals instead of amorphous-phase Co, dodecagonal quasicrystalline order is obtained, together with less-packed phases such as the $CoAg_{13}$ ($NaZn_{13}$-type), CoAg (AuCu-type), and $CoAg_3$ ($AuCu_3$-type) structures. On increasing temperature to 65 °C, 9 nm *hcp* Co nanocrystals become superparamagnetic, and the system yields the $CoAg_3$ ($AuCu_3$-type) and $CoAg_2$ (AlB_2-type) structures, as observed with 9 nm amorphous Co nanocrystals. Furthermore, by decreasing the Co nanocrystal size from 9 to 7 nm, stable AlB_2-type binary nanocrystal superlattices are produced, which remain independent of the crystallinity of Co nanocrystals with the superparamagnetic state.

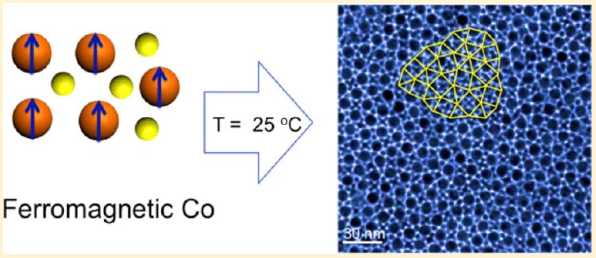

INTRODUCTION

The spontaneous assembly of uniform-sized globular entities into ordered arrays is a universal phenomenon observed for objects with diameters spanning a broad range of length scales. These extend from the atomic (10^{-8} cm), through the molecular and macromolecular with proteins, synthetic low polymers, and colloidal crystals ($\sim 10^{-6}$cm), to the wavelength of visible light ($\sim 10^{-5}$ cm). The associated concepts of sphere packing have had an influence in diverse fields ranging from pure geometrical analysis to architectural models or ideals.

During more than 200 years, a crystalline structure was based on the fact that the atomic solids are constituted of atoms assembled in 3D lattices with an invariance periodicity. In 1982, Dan Shechtman breaks the dogma on the periodicity order and proposes that some crystals can exist without 3D periodicity having a specific discrete diffraction. These specific crystals, called quasicrystals, were first discovered with intermetallic compounds.[1−3] After a long debate, the community accepted this new concept in crystallography, and Dan Shechtman was awarded the Nobel Prize in 2011.

Self-assembly of atoms, supramolecules, or nanocrystals into ordered functional superstructures is a universal process and prevalent topic in science.[4−6] The first examples of the superlattice structure in colloidal crystals were found in native gem opals containing arrays of colloidal silica spheres.[7] Furthermore, silica spheres with two different sizes in the sample of Brazilian opal can self-assemble into complex binary structures.[8] Generally, the aforementioned macroscopic particles are generally considered as hard spheres, and a superlattice formation is realized through simple entropy-driven forces.[9] Coming to the nanoscale, the formation of nanocrystal superlattices has been cultivated since the report of CdSe and Ag_2S superlattices in 1995.[10,11] This was followed by the demonstration of binary nanocrystal superlattices, which provides an open access to "metamaterials" with unique combinations of symmetry and properties not available in the single-component materials.[12,13] Previous endeavors have demonstrated that a plethora of binary structures can be produced analogous to binary atomic and ionic lattices, such as AuCu, NaCl, CsCl, AlB_2, $MgZn_2$, $MgNi_2$, $AuCu_3$, Fe_4C, $CaCu_5$, CaB_6, $NaZn_{13}$, cuboctahedra-AB_{13}, A_6B_{19}, as well as the quasicrystalline phase.[14−21] Differing from the macroscopic nanoparticles, the self-assembly of nanocrystals coated with a shell of soft matter is considered as a complex process involving the van der Waals force of inorganic cores, the van der Waals force of ligand−ligand interaction, and the surface Coulomb force,[22−25] in addition to the entropic force. Recently, quasicrystalline order was found in binary nanocrystal superlattices.[15,26] The formation of binary assemblies with dodecagonal quasicrystalline ordering in various binary nanocrystal systems, such as 13.4 nm Fe_2O_3 and 5 nm Au nanocrystals, 12.6 nm Fe_3O_4 and 4.7 nm Au nanocrystals, and 9 nm PbS and 3 nm nanocrystals, was observed. In

Received: January 15, 2015
Published: March 18, 2015

DOI: 10.1021/jacs.5b00332
J. Am. Chem. Soc. 2015, 137, 4487−4493

addition, a recent computational simulation demonstrates that the quasicrystalline phase can also be present in ordered structures assembled from tetrahedral or triangular bipyramidal building blocks.[27,28] For magnetic nanocrystals self-ordered in 3D superlattices, the interparticle interactions and consequently their magnetic interactions are significant and not trivial.[29] Furthermore, in ferro- or ferrimagnetic nanocrystals, the magnetic dipole interactions between pairs of nanocrystals influence the relaxation behavior.

Here, we present various binary systems of Co and Ag nanocrystals. Two different sizes of Co nanocrystals (9 and 7 nm) are used, differing by their crystalline structure (amorphous and *hcp*), which we refer to as nanocrystallinity (Figure 1 and Figures S1−S3, Supporting Information). Note

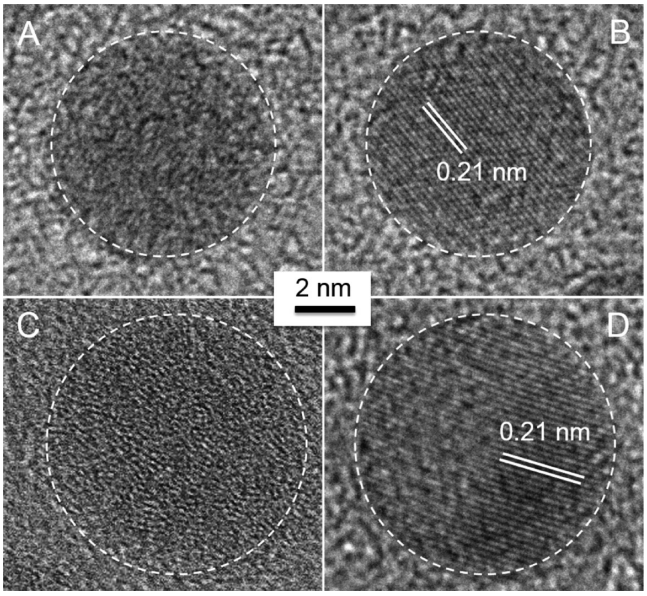

Figure 1. HRTEM images of the Co nanocrystals: (A) 7.2 nm amorphous Co; (B) 7.1 nm *hcp* Co; (C) 9.2 nm amorphous Co; and (D) 9.3 nm *hcp* Co nanocrystals.

that the *hcp* Co nanocrystals mainly consist of single domain nanocrystals, together with some polycrystalline nanocrystals.[30] Note that any crystal domains larger than 1 nm in amorphous Co nanoparticles were not observed. This rules out the possibility of crystal orientations during HRTEM observations. The 4 nm Ag nanocrystals are polycrystalline. With 7 nm Co nanocrystals, the binary systems of AlB_2 type are produced whatever the Co nanocrystallinity. In fact, both amorphous and *hcp* nanocrystals self-ordered in 3D superlattices are superparamagnetic at room temperature with a blocking temperature of 100 K (−173 °C) and 250 K (−23 °C), respectively.[30] On increasing the Co nanocrystal size to 9 nm, the magnetic interactions between ferromagnetic *hcp*-phase Co nanocrystals become of paramount importance during the self-assembly of binary nanocrystal mixtures upon solvent evaporation. The presence of magnetic interactions between *hcp* Co nanocrystals results in the formation of quasicrystalline ordering in binary nanocrystal superlattices.

RESULTS AND DISCUSSION

For all experimental data described below, the crude nanocrystals are washed four times with ethanol to remove the potential excess of free surfactant molecules to minimize the role of Coulomb forces in the assemblies described below. This is to get rid of any excess of coating agent (positively or negatively charged) in the colloidal solutions, and the Coulomb force being the major driving force to form 2D binary superlattices, rather than other relatively weaker interactions such as van der Waals forces and dipolar interparticle interactions.[31] The nanocrystals are then dispersed in toluene without any addition of excess surfactant molecules like oleic acid or dodecanethiol. The average diameters of amorphous and *hcp*-phase Co nanocrystals are, respectively, 7.2 ± 0.6 nm, 9.2 ± 0.8 nm and 7.1 ± 0.6 nm, 9.3 ± 0.8 nm, and the average diameter of Ag nanocrystals is 4.0 ± 0.4 nm. The blocking temperature, T_b, of Co supracrystals differing by their sizes and nanocrystallinity is deduced from magnetization measurements in a commercial Superconducting QUantum Interference Device (SQUID) magnetometer. For the 7.2 and 9.2 nm of amorphous Co nanoparticles, the T_b values are 100 ± 5 K (−173 ± 5 °C) and 150 ± 5K (−123 ± 5 °C), respectively, whereas for 7.1 and 9.3 nm *hcp* Co nanocrystals they are 250 ± 5K (−23 ± 5 °C) and 325 ± 5K (52 ± 5 °C), respectively (summarized in Table 1). Below T_b, the magnetocrystalline anisotropy energy dominates over the thermal energy and the nanocrystals' magnetizations are blocked along their individual "easy" axes; thus the nanocrystals enter a superferromagnetic state. Above T_b, the thermal energy is sufficient to unpin the magnetic moments from their anisotropy axes and nanocrystals enter the superparamagnetic state. Hence, both 7 nm amorphous and *hcp*-phase Co nanocrystals are in the superparamagnetic state at 25 °C, whereas 9 nm *hcp*-phase Co nanocrystals are ferromagnetic at 25 °C and reach superparamagnetic regime at 52 °C while 9 nm amorphous Co nanocrystals remain superparamagnetic at 25 °C. The effective diameter (d_{eff}), defined as the nanocrystal center-to-center distance between nanocrystals that are self-ordered in compact hexagonal networks, is determined from TEM images. The d_{eff} of Co nanocrystals with average diameters of 7.2, 9.2, and 7.1, 9.3 nm are 10.2 ± 0.9, 12.2 ± 1.1 nm and 10.3 ± 0.9, 12.1 ± 1.1 nm, respectively, whereas this diameter is 6.0 ± 0.5 nm for the 4.0 nm Ag nanocrystals. According to the hard-sphere model developed for atomic structures,[32] the system is expected to adopt the crystal structure corresponding to the most efficient space filling, to reach the maximization of the packing density, ρ, for a given ratio of the sphere radii γ, defined as the effective diameter ratio of Ag to Co nanocrystals (γ =

Table 1. Summary of the Co Nanocrystals Differing by Their Crystallinities and the Binary Structures Formed from Co and Ag Binary Mixtures

Co nanocrystallinity	diameters d/nm	size distributions/%	T_b/°C	Co/Ag binary structures/25 °C	Co/Ag binary structures/65 °C
amorphous	7.2	9	−173 ± 5	AlB_2	AlB_2
amorphous	9.2	9	−123 ± 5	NaCl	AlB_2 + $AuCu_3$
hcp	7.1	9	−23 ± 5	AlB_2	AlB_2
hcp	9.3	9	52 ± 5	quasicrystals + $NaZn_{13}$ + AuCu + $AuCu_3$	AlB_2 + $AuCu_3$ + Fe_4C

DOI: 10.1021/jacs.5b00332
J. Am. Chem. Soc. 2015, 137, 4487−4493

d_{Ageff}/d_{Coeff}). Therefore, space-filling curves plotting the packing density ρ versus ratio of the sphere radii γ provide a good estimate for entropic contributions (Figure S4, Supporting Information).[21,32] Here, with 7.2 nm Co (amorphous or *hcp*) and 4.0 nm Ag nanocrystals, γ is around 0.59, whereas with 9.2 nm Co (amorphous) and 9.3 nm Co (*hcp*) it is 0.49.

Let us consider the binary nanocrystal superlattices assembled from 7 nm Co nanocrystals differing by their crystallinity and 4 nm Ag nanocrystals. A colloidal solution of 40 μL with an initial concentration ratio of [Co]/[Ag] equal to 1/2 ([Co] = 5.8×10^{-7} M) was deposited on a TEM grid. Figure 2 shows the TEM images of the observed AlB_2-type binary superlattices for both the amorphous (Figure 2A) and the *hcp*-phase Co (Figure 2C). The preferential orientation of the AlB_2 structure has the (001) plane parallel to the substrate as is observed in the TEM images (Figure 2A and C) and FFT patterns (Figure 2B and D). The nature of the nanocrystallinity of Co nanocrystals in binary superlattices can be verified by HRTEM (Figure S5, Supporting Information), from which typical lattice fringes of *hcp*-phase Co nanocrystals with single domains can be well observed. The superlattices are demonstrated to be long-range ordered with a coherence length up to tens of micrometers (Figure 2E). To assign the nanocrystals ordering to a certain type of crystallographic space group, elemental analysis using energy dispersive X-ray spectroscopy (EDS) was further carried out (Figure S6, Supporting Information). On the basis of the several different sites of interest, the Co/Ag particles ratio was calculated to be 1/2.07, matching well with the stoichiometry of an AlB_2-type structure. These data clearly show that the change in nanocrystallinity of Co nanocrystals does not modify the AlB_2-type $Co(Ag)_2$ structures. As mentioned in this case, with a γ value of 0.59, the AlB_2-type is the most favorable structure because ρ (0.76) is larger than 0.7405 (the value for the dense packing of single-component particles). These results clearly show that the nanocrystallinity of 7 nm Co nanocrystals does not play any role during the growth of binary nanocrystal superlattices at 25 °C, for which both the amorphous and the *hcp*-phase Co nanocrystals are in a superparamagnetic state. A previous report revealed that the temperature can be a powerful structure-directing factor during the binary nanocrystal growth.[33] Nevertheless, on increasing the temperature to 65 °C for the assembly of 7 nm Co and 4 nm Ag nanocrystals, the same AlB_2-type binary nanocrystal superlattices can be observed for both amorphous and *hcp*-phase Co nanocrystals. Overall, the temperature and the nanocrystallinity of 7 nm Co nanocrystals are little effective in tuning the structures of binary nanocrystal superlattices in this case. On increasing the amount of materials and replacing TEM grid by silicon wafer, while keeping the same experimental conditions as described above, thick film was produced. High-resolution scanning electron microscopy (HRSEM) image reveals, as observed with thin film, a hexagonal stacking, where each Co nanocrystal is surrounded by six Ag nanocrystals (Figure S7, Supporting Information). This clearly shows that the AlB_2-type $CoAg_2$ structure is produced both in thin and in thick films.

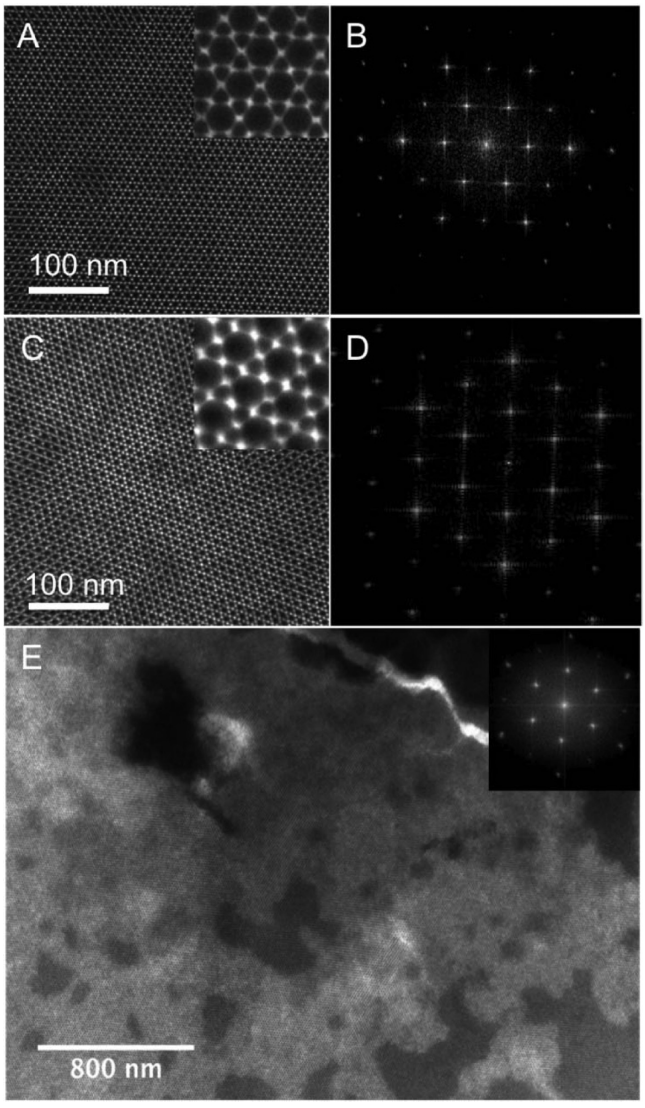

Figure 2. TEM images of binary nanocrystal superlattices assembled from 7 nm Co nanocrystals differing by their crystallinity and 4 nm Ag nanocrystals: (A) 7 nm amorphous-phase Co nanoparticles; (C) 7 nm *hcp*-phase Co nanocrystals; (B) and (D) are the FFT patterns from the corresponding TEM images (A) and (C); (E) long-range ordered AlB_2-type binary superlattices assembled from 7 nm amorphous-phase Co and 4 nm Ag nanocrystals. Inset in (E) is the corresponding FFT pattern.

By replacing the 7 nm Co nanocrystals by 9 nm nanocrystals and keeping the 4 nm Ag nanocrystals, binary superlattices are produced at 25 °C. Amorphous Co nanoparticles are characterized by an average diameter of 9.2 nm, whereas the *hcp* counterpart is 9.3 nm with an average size distribution of 9% for both (Table 1 and Supporting Information Figure S2). The experimental conditions remain the same as described above. Hence, 40 μL of a colloidal solution with an initial concentration ratio of [Co]/[Ag] equal to 1/2 ([Co] = 5.8×10^{-7} M) was deposited on a TEM grid. As shown in Figure 3, with amorphous-phase Co nanoparticles, there is an assembly of the binary mixture under quasi-equilibrium conditions. Large triangle-shaped domains with the edge length up to 20 μm are observed in Figure 3A. A further investigation into such triangular shaped domains was carried out (Figure 3B–D), and it reveals that the large Co nanocrystals are ordered into hexagonal patterns, and the smaller Ag nanocrystals are located in the vacancies between Co nanoparticles, isostructural with NaCl (space group *Fm*3*m*, 225). The preferential crystal orientation has the $(111)_{SL}$ plane parallel to the substrate, and the NaCl-type is the only binary structure that is formed under such conditions. This agrees perfectly with the hard-sphere

DOI: 10.1021/jacs.5b00332
J. Am. Chem. Soc. 2015, 137, 4487–4493

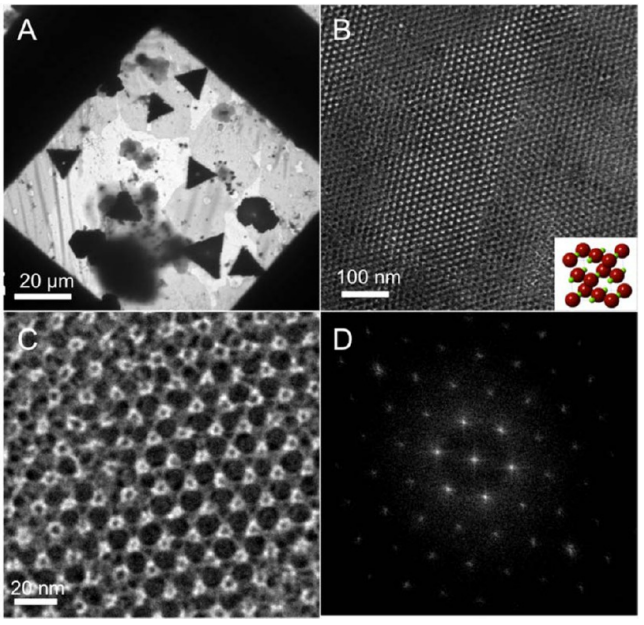

Figure 3. TEM images of binary nanocrystal superlattices assembled from amorphous 9 nm Co nanoparticles and 4 nm Ag nanocrystals: (A) low-magnification image; (B) and (C) high magnification images; (D) is the FFT pattern taken from panel (B).

model from which such a structure is expected with $\gamma = 0.49$, giving rise to a packing density $\rho \approx 0.71$. Here, because of the face-centered cubic (*fcc*) feature of NaCl-type superlattices, the mode of mesoscale superlattice growth is similar to the growth of *fcc* superlattices of single component nanocrystals, falling into the regime of the layer-by-layer crystal growth.[34] Although shaped binary supracrystals have been realized through the surface electric design of nanocrystals,[23] spontaneous growth of shaped binary supracrystals is still challenging.

With 9.3 nm *hcp* Co nanocrystals and 4.0 nm Ag nanocrystals keeping the other parameters constant, various binary superlattices are observed. One observes the formation of Co/Ag (AuCu-type, space group *P*4/*mmm*, 123) with a $(100)_{SL}$ crystal plane, or of $CoAg_3$ ($AuCu_3$-type, space group $Pm\bar{3}m$, 221) with $(100)_{SL}$ crystal plane and quasicrystalline ordering (Figures S8−S11, Supporting Information). Figure 4A shows TEM images of the asymmetric ordering of the nanocrystals. The fast Fourier transform (FFT) pattern (Figure 4B) with 12-fold symmetry agrees with the results in the literature, confirming its dodecagonal quasicrystalline ordering.[15,26] In a careful study of the TEM grid, small fractions of $CoAg_{13}$ ($NaZn_{13}$-type structures, space group $Fm\bar{3}c$, 226) are also observed in Figure 4C (Figures S9 and S10, Supporting Information). In the $CoAg_{13}$-type structure, a small 9.3 nm Co nanocrystal is surrounded by 12 other 4.0 nm Ag nanocrystals, each at the vertices of a slightly distorted icosahedron, and these icosahedral particle clusters are inserted into the cubic lattices of large 9.3 nm Co nanocrystals as observed previously.[35] Hence, the straight lines connecting the centers of Co nanocrystals in the $CoAg_{13}$ structures result in periodic squares (Figure 4C). Note that the small domains with $CoAg_{13}$ structures are isolated from the quasicrystal domains with smooth interfaces, which is not frequently discerned. At the interface between quasicrystals and $CoAg_{13}$ supracrystals, point defects are commonly observed. The data described above clearly show an abrupt difference in the binary superlattices with the Co nanocrystallinity. Note that a much more stable phase with a higher packing density such as the CoAg (NaCl-type with $\rho \approx 0.71$) structure is not detected with 9.3 nm *hcp* Co nanocrystals at $\gamma = 0.49$, whereas it is with amorphous-phase Co nanocrystals. Instead, the CoAg (AuCu-type), $CoAg_3$

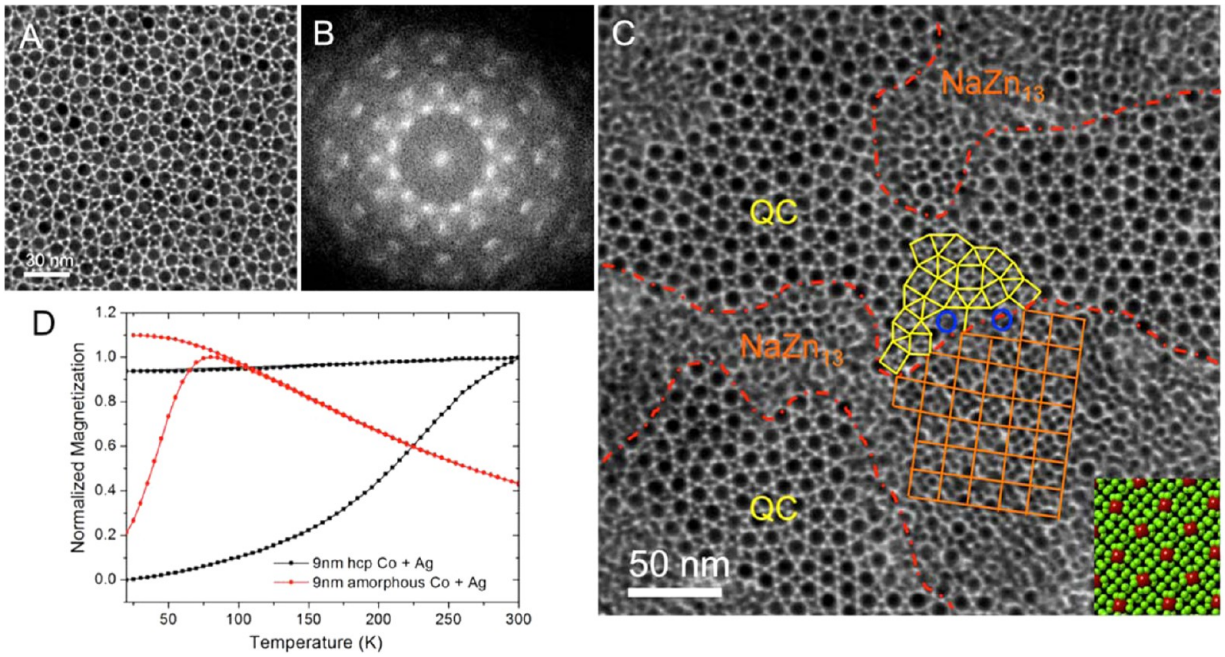

Figure 4. (A) TEM images of quasicrystalline ordering assembled from *hcp*-phase 9 nm Co nanocrystals and 4 nm Ag nanocrystals; (B) FFT pattern of the quasicrystalline superlattice; (C) transition from the quasicrystalline phase to the $NaZn_{13}$-type binary superlattice in the presence of the point defects (cycles); and (D) ZFC/FC curves of the mixture of 9 nm Co nanocrystals differing by their nanocrystallinity and 4 nm Ag nanocrystals. Inset in (C) is the model of (100) plane of $NaZn_{13}$ structure.

DOI: 10.1021/jacs.5b00332
J. Am. Chem. Soc. 2015, 137, 4487−4493

($AuCu_3$-type), $CoAg_{13}$ ($NaZn_{13}$-type), as well as the aperiodic quasicrystalline phases are generated. We know this latter quasicrystalline phase is rare, not only in atomic solids but also in binary nanocrystal superlattices. Here, the major difference between amorphous and *hcp*-phase Co nanocrystals lies in their magnetic properties, which are highly dependent on the nanocrystallinity within the same nanocrystal size. The zero field cooled/field cooled (ZFC/FC) magnetization curves for both binary samples, shown in Figure 4D, of either 9.2 nm amorphous or 9.3 nm *hcp* Co-nanocrystals and 4.0 nm Ag nanocrystals were recorded to determine their blocking temperature (T_b). Figure 4D shows that for binary systems of CoAg with amorphous Co nanocrystals T_b is 80 K (−193 ± 5 °C), whereas for *hcp* Co/Ag characterized by several structures (CoAg, $CoAg_3$, $CoAg_{13}$, and the aperiodic quasicrystalline phases) T_b is around 300 ± 5 K (25 ± 5 °C). These T_b values are slightly smaller than those obtained for amorphous (150 ± 5 K) and *hcp* (325 ± 5 K) Co nanocrystals self-assembled in 3D superlattices in the absence of Ag nanocrystals. This is attributed to the fact that the distance between Co nanocrystals in binary superlattices (5 nm) increases as compared to what is observed with one component (3 nm).[36]

The same experiments as described above were performed at 65 °C instead of 25 °C. In this case, both amorphous and *hcp* 9.3 nm Co nanocrystals are in the superparamagnetic state. A mixed colloidal solution of Co and Ag nanocrystals was heated to 65 °C and deposited at this temperature. For the 9.2 nm amorphous Co nanocrystals, $CoAg_3$ ($AuCu_3$-type) (Figure S12, Supporting Information) and $CoAg_2$ (AlB_2-type) binary nanocrystal superlattices (Figure 5A and C) are the dominant

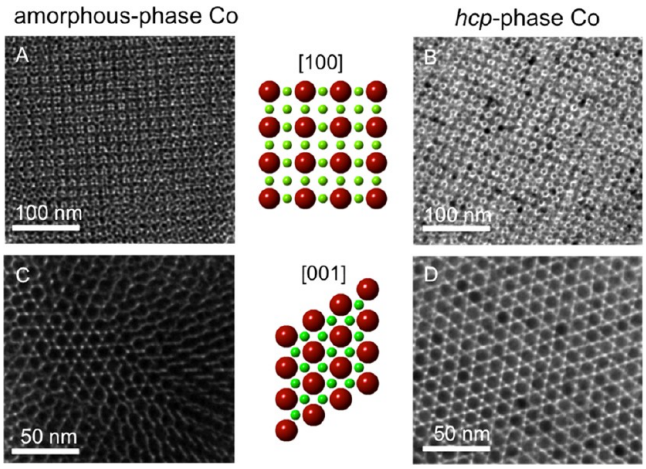

Figure 5. TEM images of binary nanocrystal superlattices assembled from 9 nm Co nanocrystals differing by their crystallinity and 4 nm Ag nanocrystals: (A and C) amorphous-phase Co nanoparticles; (B and D) *hcp*-phase Co nanocrystals.

structures instead of the NaCl-type at 25 °C. This clearly confirms, apart from the size ratio γ, that the energetic factor, that is, the deposition temperature, plays a role during the growth of binary nanocrystal superlattices. For 9.3 nm *hcp* Co nanocrystals, a $CoAg_3$ ($AuCu_3$-type) structure (Figure 5B) is the main structure with small domains of $CoAg_2$ (AlB_2-type) (Figure 5D) and $CoAg_4$ (AB_4-type structures) (Figure S13, Supporting Information). It needs to be pointed out that neither the quasicrystalline order nor the $CoAg_{13}$ ($NaZn_{13}$-type) structure is observed after careful TEM analysis. Hence, the loss of the ferromagnetic state in 9.3 nm *hcp* Co nanocrystals by increasing the temperature above T_b would result in the driving force for forming binary structures of the same magnitude, comparing the *hcp* phase with amorphous Co nanocrystals. At this stage, it is demonstrated that Co nanocrystals' magnetic state (superpara- or ferromagnetic) plays a crucial role during the growth of binary nanocrystal superlattices. Hence, in the superparamagnetic regime of Co nanocrystals, the binary structures remain quasi unaltered with the change of nanocrystallinity of Co nanocrystals, whereas quasi-crystalline ordering is observed with ferromagnetic Co nanocrystals. The aforementioned quasicrystal assemblies produced with ferromagnetic binary superlattices are not expected to be produced. In general, quasicrystal growth at the atomic scale is driven by the sum of energetic (ΔH) and entropic ($T\Delta S$) contributions, the energy-driven quasiperiodic tiling models and the entropy-driven random tiling models.[37] The reported driving force for the formation of quasicrystalline structures in binary nanocrystal superlattices is mainly attributed to entropy, as a result of maximizing the packing density ρ. The observed quasicrystalline structures combine the elements of AlB_2 and CaB_6 packing, and the size ratio γ was designed to be $\gamma = 0.43$, where the $\rho(\gamma)$ curves for the AlB_2 and CaB_6 phases cross, giving a maximum $\rho \approx 0.70$.[15] Thus, the reported quasicrystalline structures were formed under entropy-driven conditions, which allow nanocrystals to be attached randomly to the nucleus with some probability. Here, the production of quasicrystalline structure is observed for $\gamma = 0.49$ (for 9.3 nm *hcp* Co and 4 nm Ag nanocrystal). This γ value is not consistent with that reported ($\gamma = 0.43$) corresponding to the maximum probability to produce quasicrystalline structure.[15] Furthermore, the coexistent phase with a similar probability, either $CoAg_2$ (AlB_2-type) or $CoAg_6$ (CaB_6-type), cannot be detected after careful TEM analysis, whereas $CoAg_3$ ($AuCu_3$-type) and $CoAg_{13}$ ($NaZn_{13}$-type) structures having lower packing densities ρ of 0.60 and 0.68, respectively (Figure 4C and Supporting Information Figures S8−S10), are produced. Thus, the formation of quasicrystalline order cannot be simply attributed to the entropic force. In other words, the energetic contribution (ΔH), which relies on "matching rules" to dictate how nanocrystal clusters attach to the nucleus, is nontrivial in the present system, probably even being greater than the entropic ($T\Delta S$) contribution. Previous studies on semiconductor−semiconductor and semiconductor−metal binary systems have demonstrated that various forces, such as Coulombic force (U_C), van der Waals interaction between nanocrystal inorganic cores (U_{VDW}), and van der Waals interaction between ligand molecules (U_{LL}), play an energetic role during the self-assembly process.[17,22] As mentioned above, the nanocrystals were washed several times to remove any residual surfactant molecules such as either oleic acid or dodecanethiol. Moreover, neither of them was added to the colloidal solution before deposition as already described by a large number of studies on the assembly of binary nanocrystal superlattices.[31] Even though the ligand−ligand interactions (U_{LL}) remain an open question,[38] for the same coating agents and inorganic cores, in the first approximation, we would expect to have similar interactions. This is well demonstrated by the fact that with a 7 nm Co and 4 nm Ag nanocrystal system at 25 °C and a 9 nm Co and 4 nm Ag system at 65 °C, the same binary structures are produced, whatever the nanocrystallinity of Co nanocrystals. Hence, by using superparamagnetic Co nanocrystals, the forces involved in the formation of binary systems with Co nanocrystals differing by their nanocrystallinity

DOI: 10.1021/jacs.5b00332
J. Am. Chem. Soc. 2015, 137, 4487−4493

remain similar. The average diameter of nanocrystals and consequently the number of ligand per nanocrystal remain unchanged. Consequently, the van der Waals interaction energy involved is expected to be unchanged, and U_{VDW} is expected to have the same magnitude. The only difference observed at 25 °C between binary assemblies (9 nm Co and 4 nm Ag nanocrystals) produced with either amorphous or *hcp* Co nanocrystals is related to the change in the Co nanocrystal interactions due to the change in the nanocrystallinity. As mentioned above, the binary structure produced with *hcp* Co nanocrystals is ferromagnetic at 25 °C, whereas it is not with amorphous Co nanoparticles. Hence, the magnetic interactions of the inorganic cores have to be considered as another parameter in the energetic contribution, which is driven by dipolar interactions for the spherical nanocrystals.[24] Such a claim is highly supported by the fact that at 65 °C both amorphous-phase and *hcp* Co nanocrystals are in superparamagnetic states, and both give rise to the $CoAg_3$ ($AuCu_3$-type) with small domain $CoAg_2$ (AlB_2-type) binary structures. Hence, due to the drastic decrease of the force of magnetic interaction by increasing the temperature above the blocking temperature of Co nanocrystals, binary structures assembled from both amorphous-phase and *hcp* Co nanocrystals and Ag nanocrystals are mainly driven by the sum of van der Waals forces as well as of the entropic term. These results permit one to conclude that magnetic interactions between ferromagnetic nanocrystals are the key parameter in producing quasicrystalline structure of nanocrystals (see the Supporting Information).

It needs to be pointed out that the strong magnetic interactions are still present in 9 nm *hcp* Co nanocrystals when they are used to grow single component superlattices at low temperature (25 °C). The result shows that a large domain of disordered structure accompanied by small domains of ordered structure presents on the copper grid for 9 nm *hcp* Co nanocrystals, whereas a large domain of ordered face-centered cubic (fcc) structure presents on increasing the temperature to 65 °C (Figure 6). This suggests that the magnetic interactions between nanocrystals can lead to the local agglomeration of Co nanocrystals preventing formation of densely packed ordered structure with high filling factor.

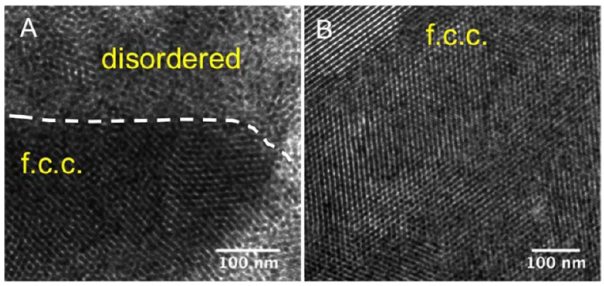

Figure 6. TEM images of the assemblies of single component 9.3 nm *hcp* Co nanocrystals: (A) at 25 °C; (B) at 65 °C.

CONCLUSIONS

In summary, we conclude that the nanocrystallinity of supraparamagnetic Co nanocrystals does not play any role in the Co/Ag binary nanocrystal superlattices, whereas for ferromagnetic Co nanocrystals, the additional strong magnetic interactions between the ferromagnetic nanocrystals with fixed spins in the system locally stabilize quasicrystalline and $CoAg_{13}$ structures. The energetic contribution of magnetic interactions is dominant during the coassembly of binary nanocrystal mixtures where ferromagnetic nanocrystals are involved, while the magnetic interaction between the superparamagnetic nanocrystals is relatively weak, and the hard-sphere interactions remain an important factor for this case.

ASSOCIATED CONTENT

Supporting Information

Size histograms of the nanocrystals, TEM, HRTEM, and HRESM images of the binary nanocrystal superlattices, and EDS analysis of the binary nanocrystal superlattices. This material is available free of charge via the Internet at http://pubs.acs.org.

AUTHOR INFORMATION

Corresponding Author

*mppileni@orange.fr

Notes

The authors declare no competing financial interest.

ACKNOWLEDGMENTS

The research leading to these results has been supported by an Advanced Grant of the European Research Council under Grant 267129. We thank Dr. Khashayar Khazen for the measurement of magnetic properties. We thank Mr. Alan Boyd for the correction of the language. Z.Y. and J.W. thank the China Scholarship Council for financial support.

REFERENCES

(1) Shechtman, D.; Blech, I.; Gratias, D.; Cahn, J. W. *Phys. Rev. Lett.* **1984**, *53*, 1951−1953.
(2) Levine, D.; Steinhardt, P. J. *Phys. Rev. Lett.* **1984**, *53*, 2477−2480.
(3) Ishimasa, T.; Nissen, H. U.; Fukano, Y. *Phys. Rev. Lett.* **1985**, *55*, 511−513.
(4) Wang, T.; Zhuang, J. Q.; Lynch, J.; Chen, O.; Wang, Z. L.; Wang, X. R.; LaMontagne, D.; Wu, H. M.; Wang, Z. W.; Cao, Y. C. *Science* **2012**, *338*, 358−363.
(5) Nie, Z.; Petukhova, A.; Kumacheva, E. *Nat. Nanotechnol.* **2010**, *5*, 15−25.
(6) Talapin, D. V. *ACS Nano* **2008**, *2*, 1097−1100.
(7) Sanders, J. V. *Nature* **1964**, *204*, 1151−1153.
(8) Sanders, J. V. *Philos. Mag. A* **1980**, *4*, 705−720.
(9) Eldridge, M. D.; Madden, P. A.; Frenkel, D. *Nature* **1993**, *365*, 35−37.
(10) Motte, L.; Billoudet, F.; Pileni, M. P. *J. Phys. Chem.* **1995**, *99*, 16425−16429.
(11) Murray, C. B.; Kagan, C. R.; Bawendi, M. G. *Science* **1995**, *270*, 1335−1338.
(12) Kiely, C. J.; Fink, J.; Brust, M.; Bethell, D.; Schiffrin, D. J. *Nature* **1998**, *396*, 444−446.
(13) Redl, F. X.; Cho, K. S.; Murray, C. B.; O'Brien, S. *Nature* **2003**, *423*, 968−971.
(14) Shevchenko, E. V.; Talapin, D. V.; Murray, C. B.; O'Brien, S. *J. Am. Chem. Soc.* **2006**, *128*, 3620−3637.
(15) Talapin, D. V.; Shevchenko, E. V.; Bodnarchuk, M. I.; Ye, X.; Chen, J.; Murray, C. B. *Nature* **2009**, *461*, 964−967.
(16) Cheon, J.; Park, J. I.; Choi, J. S.; Jun, Y. W.; Kim, S.; Kim, M. G.; Kim, Y. M.; Kim, Y. J. *Proc. Natl. Acad. Sci. U.S.A.* **2006**, *103*, 3023−3027.
(17) Shevchenko, E. V.; Talapin, D. V.; Kotov, N. A.; O'Brien, S.; Murray, C. B. *Nature* **2006**, *439*, 55−59.
(18) Evers, W. H.; Friedrich, H.; Filion, L.; Dijkstra, M.; Vanmaekelbergh, D. *Angew. Chem., Int. Ed.* **2009**, *48*, 9655−9657.

DOI: 10.1021/jacs.5b00332
J. Am. Chem. Soc. 2015, 137, 4487−4493

(19) Dong, A.; Chen, J.; Vora, P. M.; Kikkawa, J. M.; Murray, C. B. *Nature* **2010**, *466*, 474−477.
(20) Boneschanscher, M. P.; Evers, W. H.; Qi, W.; Meeldijk, J. D.; Dijkstra, M.; Vanmaekelbergh, D. *Nano Lett.* **2013**, *13*, 1312−1316.
(21) Ye, X.; Chen, J.; Murray, C. B. *J. Am. Chem. Soc.* **2011**, *133*, 2613−2620.
(22) Chen, Z.; Moore, J.; Radtke, G.; Sirringhaus, H.; O'Brien, S. *J. Am. Chem. Soc.* **2007**, *129*, 15702−15709.
(23) Kalsin, A.; Fialkowski, M.; Paszewski, M.; Smoukov, S. K.; Bishop, K. J. M.; Grzybowski, B. A. *Science* **2006**, *312*, 420−424.
(24) Bishop, K. J. M.; Wilmer, C. E.; Soh, S.; Grzybowski, B. A. *Small* **2009**, *5*, 1600−1630.
(25) Nagaoka, Y.; Chen, O.; Wang, Z.; Cao, Y. C. *J. Am. Chem. Soc.* **2012**, *134*, 2868−2871.
(26) Bodnarchuk, M. I.; Erni, R.; Krumeich, F.; Kovalenko, M. V. *Nano Lett.* **2013**, *13*, 1699−1705.
(27) Haji-Akbari, A.; Engel, M.; Keys, A. S.; Zheng, X.; Petschek, R. G.; Palffy-Muhoray, P.; Glotzer, S. C. *Nature* **2009**, *462*, 773−777.
(28) Haji-Akbari, A.; Engel, M.; Glotzer, S. C. *Phys. Rev. Lett.* **2011**, *107*, 215702.
(29) Jun, Y. W.; Seo, J. W.; Cheon, J. *Acc. Chem. Res.* **2008**, *41*, 179−189.
(30) Yang, Z.; Cavalier, M.; Walls, M.; Bonville, P.; Pileni, M. P. *J. Phys. Chem. C* **2012**, *116*, 15723−15730.
(31) Sun, Z.; Luo, Z.; Fang, J. *ACS Nano* **2010**, *4*, 1821−1828.
(32) Parthe, E. *Z. Kristallogr.* **1961**, *115*, 52−79.
(33) Bodnarchuk, M. I.; Kovalenko, M. V.; Heiss, W.; Talapin, D. V. *J. Am. Chem. Soc.* **2010**, *132*, 11967−11977.
(34) Wan, Y. F.; Goubet, N.; Albouy, P. A.; Pileni, M. P. *Langmuir* **2013**, *29*, 7456−7463.
(35) Shevchenko, E. V.; Talapin, D. V.; O'Brien, S.; Murray, C. B. *J. Am. Chem. Soc.* **2005**, *127*, 8741−8747.
(36) Yang, Z.; Wei, J.; Bonville, P.; Pileni, M. P., unpublished results.
(37) Keys, A. S.; Glotzer, S. C. *Phys. Rev. Lett.* **2007**, *99*, 235503.
(38) Wan, Y.; Goubet, N.; Albouy, P.-A.; Schaeffer, N.; Pileni, M.-P. *Langmuir* **2013**, *29*, 13576−13581.

DOI: 10.1021/jacs.5b00332
J. Am. Chem. Soc. 2015, 137, 4487−4493